International Journal of Robotics and Control Systems
Vol. 5, No. 1, 2025, pp. 311-332
ISSN 2775-2658
http://pubs2.ascee.org/index.php/ijrcs

Mitigating Subsynchronous Resonance in Doubly Fed Wind Turbine Induction Generator Using FACTS Devices: A Comparative Case Study

Bui Thi Hoa Phuong [a,1], Tran Thanh Ngoc [a,2], Pham Hong Thanh [b,3], Le Van Dai [a,4,*]

[a] Electric Power System Research Group, Faculty of Electrical Engineering Technology, Industrial University of Ho Chi Minh City, Ho Chi Minh City and 70000, Viet Nam
[b] Institute of Engineering and Technology, Thu Dau Mot University, Binh Duong Province and 820000, Viet Nam
[1] 21141661.phuong@student.iuh.edu.vn; [2] tranthanhngoc@iuh.edu.vn; [3] thanhph@tdmu.edu.vn; [4] levandai@iuh.edu.vn
* Corresponding Author

ARTICLE INFO

Article history
Received May 07, 2024
Revised December 11, 2024
Accepted December 24, 2024

Keywords
Sub-Synchronous Resonance (SSR);
Flexible AC Transmission System (FACTS);
The IEEE First Benchmark Model (FBM);
Double-Fed Induction Generator (DFIG);
Wind Turbine

ABSTRACT

Sub-synchronous resonance (SSR) may result from the recent integration of wind power generating systems (WPGS) based on double-fed induction generators (DFIG) into weak grids using long transmission lines with series capacitor adjustment. The amount of series compensation used in the transmission line determines how much SSR affects the grid, which may lead to serious instability. Flexible alternating current transmission system (FACTS) devices, which aid in controlling and stabilizing grid oscillations, are a workable way to lessen the impacts of SSR. In order to analyze the efficacy of FACTS controllers in mitigating SSR, this work examines the modeling and control techniques of WPGS-DFIG employing Thyristor controlled series capacitor (TCSC), static Var compensator (SVC), and static synchronous compensator (STATCOM). Time-domain simulations on a modified IEEE First benchmark, with varying series compensation levels and grid fault circumstances, are used to verify the study's correctness and effectiveness. According to the simulation findings, the STATCOM controller mitigates SSR far more effectively than TCSC and SVC. The STATCOM controller optimizes the performance of the WPGS-DFIG system by increasing dynamic responsiveness and grid stability in SSR-prone conditions.

1. Introduction

Wind energy has rapidly developed in recent years due to the increasing demand for energy and the escalating environmental pollution issue [1]. Wind power plants are often located far from population centers to minimize the impact on residential areas [2], [3]. Consequently, transmitting electrical energy over long distances inevitably results in power and voltage losses. To address this issue, fixed series capacitors (FSC) are installed on transmission lines from wind power plants to load centers to increase the transmission capacity of the lines. However, in certain cases, FSC may interact with the doubly fed induction generator (DFIG) of wind turbines, one of today's most common types of wind turbine generators. This interaction can lead to the risk of SSR [4], [5].

The phenomenon of SSR occurs in one of three forms: induction generator effect (IGE), torsional interaction (TI), and transient torque (TT). The TI rarely occurs in wind power plants using DFIG

due to the low stiffness of the wind turbine blades, as mentioned in [6], [7]. The main reasons for SSR in these plants are IGE and TT, as introduced by authors in [3], [8]. The first occurrence of SSR in a wind power system occurred in 2009 at a wind power plant in southern Texas, USA. The cause was the connection of the wind power plant to a fixed series capacitor, and the oscillation frequency was 20Hz. The issue was resolved by disconnecting the capacitor from the transmission line as in [4], [9], but it is not the best solution. Another incident occurred at a wind power plant in southern China in 2012, where the oscillation frequency was in the range of from 6 Hz to 8 Hz. This incident led to the shutdown of many wind turbines [3]. An example of cracks on No.7 journal of Unit-1 generator of the Vung Ang thermal power plant in Viet Nam, Nov. 2015, due to the SSR phenomenon occurring shown in Fig. 1, [10].

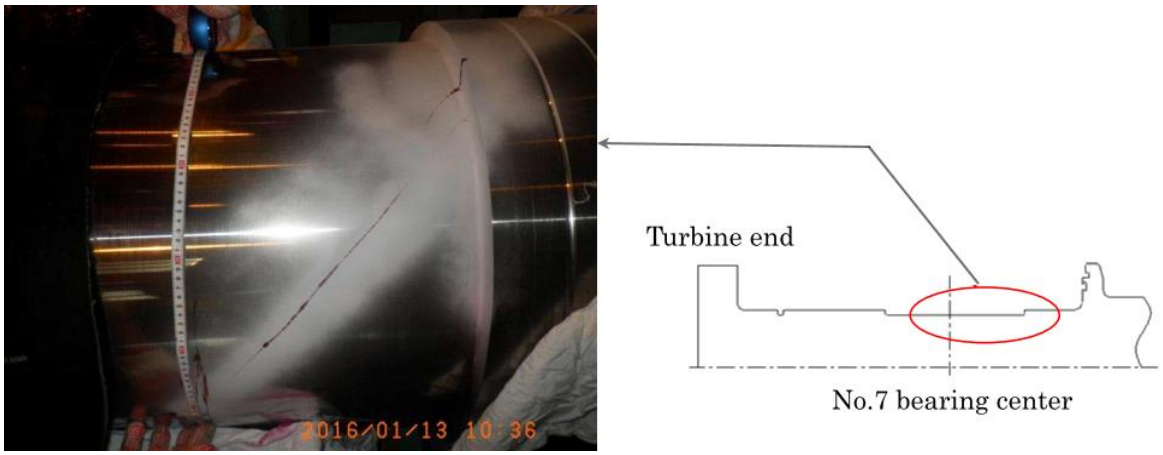

Fig. 1. Crack on the Unit-1 generator rotor of the vung ang thermal power plant, Vietnam, November 2015, caused by the SSR phenomenon

With the recent advancement in power electronics, the use of FACTS in power systems is becoming increasingly common. FACTS devices have the capability to rapidly control the parameters of the electrical grid [11], [12]. This feature of FACTS devices can be harnessed to enhance voltage stability, control power flow flexibly, and potentially prevent SSR occurrences in power systems. SVC is renowned for their rapid dynamic reactive power support, which was crucial during emergency situations to prevent voltage collapse, as presented in [13], [14]. In the literatures [13], [15], authors presented the comparison analysis of FACTS controllers, including STATCOM, SVC, and TCSC, for voltage stability and power loss reduction. Besides, the impedance of transmission lines is adjusted to control power flow and dampen oscillations related to SSR by TCSC, which was present in [10], [16]. A simple sub-synchronous resonance control strategy based on an orthogonal proportional action applied to the rotor currents and a variable gain in the PI controller adjusted as a function of the DFIG rotational speed was proposed in [17]. In [18], machine parameters, especially stator winding resistance, significantly affect how wind turbines (DFIG and PMSG) handle grid faults, suggesting careful design choices can improve performance without expensive external solutions. A review of sub-synchronous resonance (SSR) in DFIG wind farms, covering its analysis methods, causes due to various DFIG parameters, and mitigation techniques using controllers, was presented in [19]. Authors in [20] proposed vector control to manage a DFIG wind turbine system, allowing for independent control of power sent to the grid despite wind speed changes. It also explains DFIG components and validates the concept through simulation. In literature, [21] presented a study that shows a control method (DPC) improves stability and efficiency in simulations, suggesting a link between control and grid conditions for better DFIG performance. E-STATCOM, which uses a super-capacitor, was proposed in [21]. The simulation results show it effectively controls system oscillations during disturbances like torque changes and short circuits, compared to no control and its control.

In this research, the author will employ typical FACTS devices such as TCSC and STATCOM to mitigate SSR phenomena in wind power systems using DFIG. The effectiveness in reducing SSR will be demonstrated through simulation results using MATLAB/Simulink under various operating

conditions. Through that, this article wants to contribute to 3-main issues: *i*) general introduction to SSR in DFIG and FSC integrated power systems; *ii*) present the FACTS devices used to resolve SSR as SVC, TCSC and STATCOM; *iii*) evaluate the effectiveness of the 3 FACTS devices commonly used in the power system mentioned above in eliminating SSR in two investigated cases: (a) changing the compensation ratio of FSC and (b) system re-stabilizing after a 3-phase fault. The results can be used as a reference criterion in the practical design, renovation, and operation of power systems for the addition of FACTS equipment.

The structure of the paper is presented as follows: Section 2 details the models of the components within the research system. A concise definition and classification of SSR phenomena are outlined in Section 3. Section 4 encompasses the structure and control system models of the TCSC, SVC, and STATCOM. In Section 5, simulation studies are conducted to verify the accuracy and effectiveness of the controller in mitigating SSR. Finally, Section 6 concludes the paper.

2. Research System Model

The research system, illustrated in Fig. 2 [22], is developed based on the IEEE First BenchMark model. This system integrates a wind power setup that employs DFIGs with a total installed capacity of 100 MW. This capacity is derived from 66 individual turbines, each having a generation capacity of 1.5 MW. These turbines are connected to the grid through an FSC that operates at a voltage level of 161 kV. In order to simplify the analysis and computational requirements, the collective operation of all wind turbines is represented by a single equivalent turbine with consolidated parameters. Several recent studies have validated This equivalent turbine approach, which confirms its effectiveness in accurately simulating the overall behavior of wind power systems of this scale [23], [24]. Capacitive series compensation is employed in this system as an economical and effective solution to enhance the power transmission capacity of long-distance transmission lines. By reducing the overall reactance of the transmission line, series capacitors improve the system's power transfer capability and voltage stability. This approach is particularly advantageous in large-scale renewable energy systems, where maximizing transmission efficiency is crucial for integrating high-capacity wind farms into the grid.

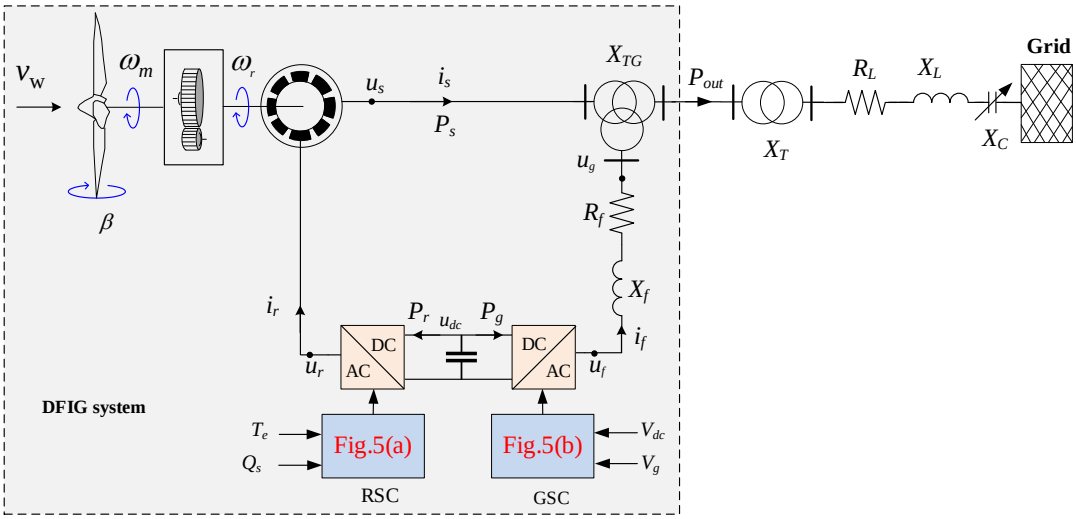

Fig. 2. Single-line model of modified IEEE first benchmark considering the DFIG system

Nevertheless, the compensation level for transmission lines linked to wind farms powered by DFIG is not adequately high. Consequently, if a DFIG-powered wind farm is connected in series with a transmission line that has capacitive series compensation, there is a heightened risk of the SSR phenomenon due to the significant inductive characteristics of DFIG. SSR occurs when a system compensated by a series capacitor exchanges significant energy with a turbine generator at a frequency lower than the synchronous frequency [25], [26].

When individual wind turbines are synthesized, the aggregate inertia increases, and the fundamental power also rises; hence, the relative inertia value of the shaft system remains unchanged. Similarly, this phenomenon occurs with other parameters, such as impedance. Therefore, the parameters of a 1.5 MW DFIG turbine within the unit system can be used for an equivalent 100 MW wind turbine generator. To comprehend this system, the next section of the paper will present the differential and algebraic equations governing the system.

2.1. Wind Turbine Aerodynamic Model

The following equation represents the mechanical torque [27], [28]:

$$T_m = \frac{1}{2\lambda}\rho A R C_p v_w^2 \tag{1}$$

where ρ is the air density, A is the swept area of the blade, R is the blade length, v_w is the wind speed, C_P is the power coefficient of the rotor and can be described by the following equation:

$$C_p = \frac{1}{2}\left(\frac{RC_f}{\lambda} - 0.022\theta - 2\right)e^{-0.255\frac{RC_f}{\lambda}} \tag{2}$$

where θ is the pitch angle, C_f is the design constant ratio of the blade cross-section and tip-speed ratio, and λ is the tip-speed ratio and can be determined as follows:

$$\lambda = \frac{\omega_m R}{v_w} \tag{3}$$

in which ω_m is the mechanical speed of the wind turbine.

2.2. Drive Train Model

The wind turbine is connected to the generator rotor by a gearbox, as shown in Fig. 2. The rotational system, consisting of the wind turbine shaft, gearbox, and generator shaft, is called the drive train system. The two-mass model is chosen to model the drive train. This system has proved sufficient for the dynamic analysis of grid-connected WT-DFIG. This paper considers the drive train model, as shown in Fig. 3. The differential equation of motion for the two degrees can be derived by applying Newton's second law of motion as follows [29]:

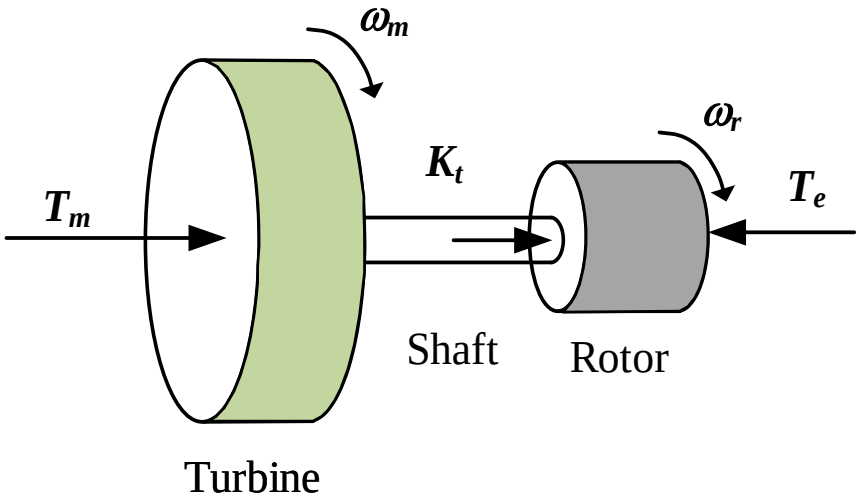

Fig. 3. Two-mass drive train model

$$\begin{cases} 2H_t\theta_1 + K_t(\theta_1 - \theta_2) = T_m \\ 2H_g\theta_2 + K_t(\theta_2 - \theta_1) = -T_e \end{cases} \tag{4}$$

in which $\theta_1 = d\omega_m/dt$ and $\theta_2 = d\omega_r/dt$ are the angle's displacements of wind turbine and generator rotors, respectively; here ω_r is the generator rotor angular speed; H_t and H_g are the wind turbine and generator inertia constants, respectively; T_m and T_e are the wind turbine mechanical torque and generator electromagnetic torque, respectively; K_t is the stiffness of the turbine shaft. Equations (1) and (4) can be rewritten under the condition of constants $H_t = H_g = H$ as follows:

$$2H(\theta_1 + \theta_2) = T_m - T_e \tag{5}$$

2.3. Induction Generator Model

The electric generator chosen for the wind energy conversion is the equivalent circuit, as shown in Fig. 4, including a WRIG with the stator windings directly connected to the grid. Meanwhile, the rotor windings are connected to a back-to-back converter with the RSC and GSC connected to a common DC-link capacitor. Thanks to the DFIG, it can generate or absorb reactive power and also supply active power to the grid. In this paper, the generator model is written in the direct and *dq* quadrature synchronous reference frame and presented by the system of the following equations [30], [31]. The stator and rotor voltages can be written as follows

$$\begin{cases} u_{sd} = R_s i_{sd} + \dfrac{d\varphi_{sd}}{dt} - \omega_s \varphi_{sq} \\ u_{sq} = R_s i_{sq} + \dfrac{d\varphi_{sq}}{dt} + \omega_s \varphi_{sd} \end{cases} \tag{6}$$

$$\begin{cases} u_{rd} = R_r i_{rd} + \dfrac{d\varphi_{rd}}{dt} - (\omega_s - \omega_r)\varphi_{sq} \\ u_{rq} = R_r i_{rq} + \dfrac{d\varphi_{rq}}{dt} + (\omega_s - \omega_r)\varphi_{rd} \end{cases} \tag{7}$$

where $u_{sd}, u_{sq}, u_{rd}, and\ u_{rq}$ are the *d*- and *q*- axes components of stator and rotor voltages, respectively; $i_{sd}, i_{sq}, i_{rd}, and\ i_{rq}$ are the *d*- and *q*- axes components of stator and rotor currents, respectively; $R_s\ and\ R_r$ are the stator and rotor resistances, respectively; $\omega_s\ and\ \omega_r$ are the angular speed of the electrical grid and the angular speed of the rotor, respectively; φ_{sd}, φ_{sd}, $\varphi_{sq}, and\ \varphi_{rd}$ are the *d*- and *q*- axes components of stator and rotor fluxes, respectively, and can be determined as.

$$\begin{cases} \varphi_{sd} = (L_{ls} + L_m) i_{sd} + L_m i_{rd} \\ \varphi_{sq} = (L_{ls} + L_m) i_{sq} + L_m i_{rq} \end{cases} \tag{8}$$

$$\begin{cases} \varphi_{rd} = (L_{lr} + L_m) i_{rd} + L_m i_{sd} \\ \varphi_{rq} = (L_{lr} + L_m) i_{rq} + L_m i_{sq} \end{cases} \tag{9}$$

where L_{ls} and L_{lr} are the stator and rotor leakage inductances, respectively, and L_m is the magnetizing inductance. The electrical torque is

$$T_e = \frac{3p}{2}\left(u_{rd} i_{rq} - u_{rq} i_{rd}\right) \tag{10}$$

The mechanical angular speed of wind turbine is

$$\omega_m = \frac{1}{J}\int (T_m - T_e) dt \tag{11}$$

where J is the total inertia and T_m is the mechanical torque. The stator's active and reactive powers are

$$\begin{cases} P_s = \frac{3}{2}(u_{sd}i_{sd} + u_{sq}i_{sq}) \\ Q_s = \frac{2}{3}(u_{sq}i_{sd} - u_{sd}i_{sq}) \end{cases} \quad (12)$$

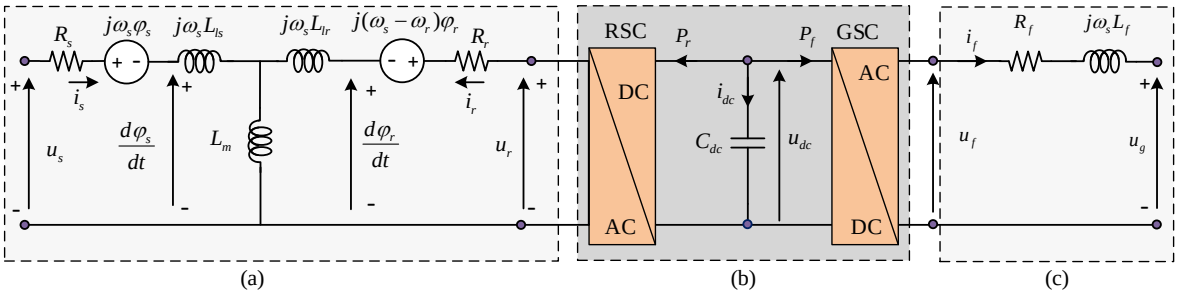

Fig. 4. Equivalent circuit of DFIG: (a) WRIG generator, (b) Power electronic converters, (c) Grid filter

2.4. DC-link Capacitor Model

The dynamic model of the DC-Link capacitor between the DFIG converters is represented by the following equations [28], [32].

$$C_{dc}u_{dc}\frac{du_{dc}}{dt} = -(P_r + P_f) \quad (13)$$

where P_r and P_f are the power flowing into the RSC and GSC, respectively; C_{dc} and u_{dc} are the DC-link capacitor and voltage, respectively.

2.5. The Grid Filter

The connection of the GSC to the network is done via a filter to attenuate the frequency of the harmonics generated by the power converter, as shown in Fig. 4. According to Kirchhoff's laws, the equations of the network-connected filter are expressed under the dq reference frame rotating at the electrical angular velocity of the grid voltage as follows.

$$\begin{cases} u_{fd} = u_{gd} - R_f i_{fd} + \omega_s L_f i_{fq} - L_f \frac{di_{fd}}{dt} \\ u_{fq} = u_{gq} - R_f i_{fq} - L_f \frac{di_{fd}}{dt} - \omega_s L_f i_{fd} \end{cases} \quad (14)$$

The power flow between the GSC and the grid is

$$\begin{cases} P_f = \frac{3}{2}(u_{fd}i_{fd} + u_{fq}i_{fq}) \\ Q_f = \frac{2}{3}(u_{fq}i_{fd} - u_{fd}i_{fq}) \end{cases} \quad (15)$$

2.6. The Control Method of WPGS-DFIG

The WPGS-DFIG is controlled based on the variable frequency converter that includes RSC and GSC controllers. The purpose of RSC is to allow separate control of active and reactive power [33]. This facilitates high flexibility, allowing DFIG to capture maximum energy from the wind and support reactive power into the grid. The main purpose of GSC is to maintain a constant voltage across the capacitor regardless of the magnitude and direction of the rotor power. The PI controller is proposed to apply the RSC and GSC, as illustrated in Fig. 5, [34]-[36]. For this paper, they are calculated and designed based on [10], [35]. For the RSC, the control structure involves the inner and outer loops, as shown in Fig. 5 (a), in which the inner one independently regulates the *d*- and *q*-

axes rotor current components, and the outer one regulates the electric torque and reactive power. For the GSC, the control structure involves the inner and outer loops, as shown in Fig. 5 (b), in which the inner one independently regulates the *d*- and *q*- axes grid current components, and the outer one regulates the DC-link and stator voltages.

3. SSR Phenomenon Analysis

The SSR is a phenomenon occurring in power systems when there is an exchange of energy between the mechanical system of the turbine generator and the electrical [37], [38]. This energy exchange happens at one or more natural frequencies of the interconnected systems. The SSR can lead to various serious issues for the power system. This excited rotor current causes asynchronous armature voltage components that can increase the asynchronous armature current height to create SSR. The main types of SSR include IGE, TI, and TT. The following sections of this research will briefly describe various types of SSR.

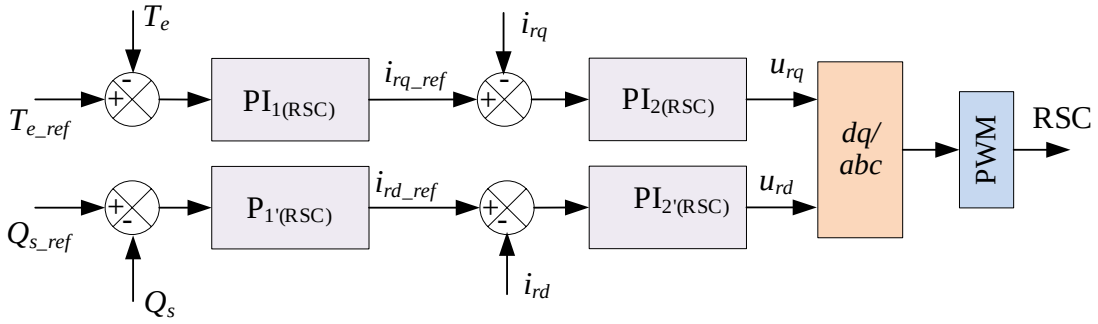

(a)

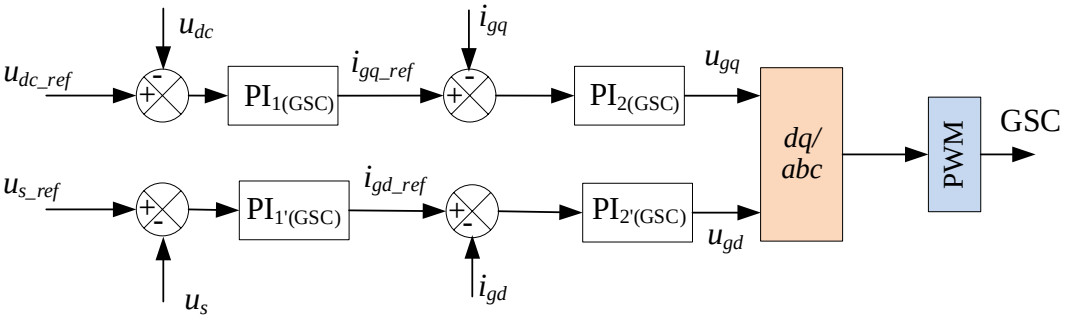

(b)

Fig. 5. The control scheme of DFIG: (a) The control scheme of RSC and (b) The control method of GSC

3.1. Torsional Interaction

The TI typically occurs when the generator generates the synchronous torque near one or more natural torsional frequencies of the wind turbine rotor shaft. Torsional interaction leads to torsional oscillations of the generator rotor, resulting in the excitation of the reactive voltage components. These reactive voltage components are generated at both above and below synchronous frequencies. Furthermore, the sub-synchronous frequency voltage is generated in a manner to sustain the synchronous torque. At this point, when the torsional torque exceeds or equals the mechanical damping factor of the oscillation system, self-excitation occurs. This phenomenon, often referred to as torsional interaction, can lead to damage to the turbine rotor shaft if not prevented in a timely manner [39], [40].

3.2. Transient Torque

The TT can be understood as forces generated from disturbances occurring in the system, such as faults, equipment switching. These system disturbances can lead to rapid and unexpected changes

in the power grid, potentially altering the natural frequencies of the network and thus affecting the system's functionality. System disturbances typically exhibit DC signals only in power transmission systems without fixed series capacitors. On the other hand, power grids utilizing fixed-series capacitors often contain one or more oscillation frequencies [39], [40]. These frequencies depend on the power grid's total capacitance, resistance, and inductance. If any of these frequencies align with the oscillation frequency of the wind turbine rotor shaft, it can significantly amplify torque amplitude. This torque, in turn, is directly proportional to the amplitude of the oscillating current. Each occurrence of excessive transient torque with a large amplitude contributes to the reduction in the lifespan of the rotor shaft due to fatigue-induced damage. If this process is not mitigated, it can severely damage the turbine rotor shaft.

3.3. Induction Generator Effect

For the SSR, the electrical and mechanical components of the turbine generator are in resonance with the next condenser. Therefore, SSR includes the mechanical and electrical parts of the power system. The shaft of the turbine generator matches its mechanical resonance to the resonance of the series capacitor when there is a radial or near-radial connection between the two. The electrical resonance frequency calling f_{er} the system in Fig. 6, can be calculated as follows

$$f_{er} = f_0 \sqrt{\frac{X_C}{\underbrace{X_{DFIG} + X_L + X_T}_{X_{Total}}}} \tag{16}$$

in which f_0 is the average frequency of the rotor; $X_g, X_L, X_T \; and \; X_C$ are the reactance of the generator, transformer, line and longitudinal capacitor, respectively. X_C can be up to 50-70% of X_{Total} value and $f_{er} < f_0$ in normally.

The presence of resonant current of frequency f_{er} generates torque and current of frequency f_r in the rotor winding, and this frequency can be calculated as follows

$$f_r = f_0 - f_{er} \tag{17}$$

At the steady-state as the equivalent circuit of in Fig. 6, the sub-synchronous slip, calling s_{er} is given by

$$s_{er} = \frac{f_n - f_r}{f_n} \tag{18}$$

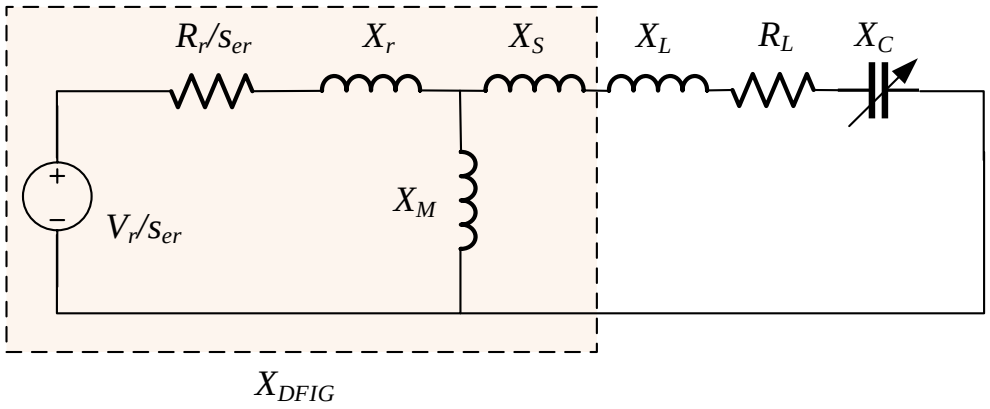

Fig. 6. The equivalent circuit of DFIG is connected to a series of compensated networks under SSR

The IGE typically occurs due to the self-excitation of the power system. According to reference [40], [41], the large rotor reactance and the synchronous current are usually negative. Additionally,

the power grid plays a crucial role in opposing these synchronous currents. On the other hand, if the negative reactance of the generator is much greater than the magnitude of the positive reactance of the power system, the synchronous current at that point becomes constant. The self-excitation phenomenon occurs, causing oscillations at synchronous frequencies in the system.

4. FACTS Devices

This paper will utilize three representative FACTS devices, including TCSC, SVC, and STATCOM, to mitigate SSR in wind power systems using DFIG turbines [42], [43]. The controllers of these FACTS devices play a crucial role in minimizing SSR in the power system to enhance stability. To understand the SSR mitigation mechanism of these FACTS devices in this study, the following will present the devices and control systems designed to reduce SSR.

4.1. TCSC

Structure and principle of operation: The TCSC is one of the most widely used series-connected FACTS devices, aiming to enhance transmission capability and improve system stability. The typical structure of TCSC is depicted in Fig. 7 and is marked in a pale yellow color [42], [44], [45]. TCSC comprises three main components: a capacitor with the capacitive reactance $X_{\mathrm{C\_tcsc}}$ connected in parallel with an inductor with the inductive reactance X_{L_tcsc}, controlled by two $T_{\mathrm{tcsc\_1}}$ and $T_{\mathrm{tcsc\_2}}$ opposing thyristors connected in parallel. The firing angles of the thyristors are controlled to regulate the electrical impedance of the TCSC according to the system's control algorithm [44], [46], [47].

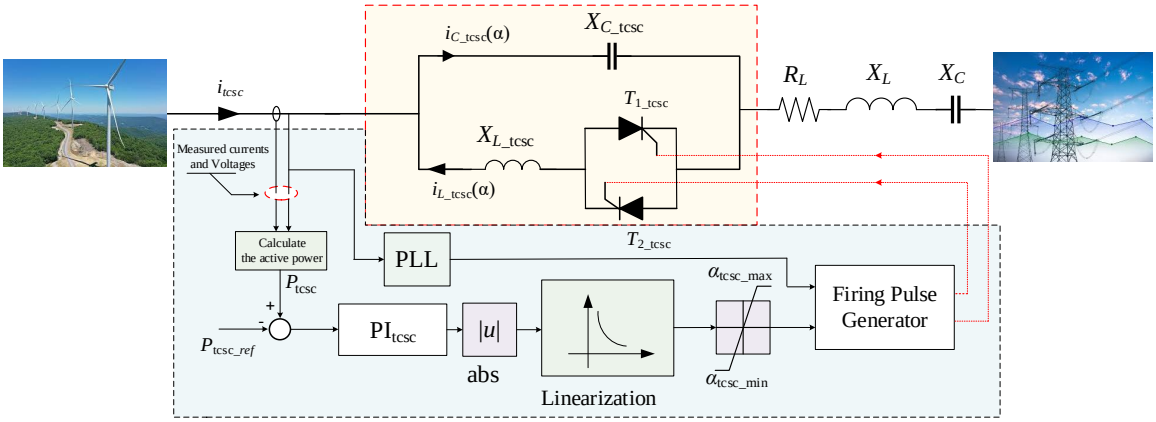

Fig. 7. The configuration and control method of TCSC

TCSC can be controlled to operate in either the capacitive or inductive regions, avoiding the resonance region. The relationship between the firing angle and $X_{\mathrm{tcsc}}$is described as follows.

$$X_{\mathrm{tcsc}} = X_{\mathrm{C\_tcsc}} - \left(\frac{X_{\mathrm{C\_tcsc}}^2}{X_{\mathrm{C\_tcsc}} - X_{L\_\mathrm{tcsc}}}\right)\left(\frac{2\beta_{\mathrm{tcsc}} + sin(2\beta_{\mathrm{tcsc}})}{\pi}\right) + \left(\frac{4X_{\mathrm{C\_tcsc}}^2}{X_{\mathrm{C\_tcsc}} - X_{L\_\mathrm{tcsc}}}\frac{cos^2\beta_{\mathrm{tcsc}}}{k_{\mathrm{tcsc}}^2 - 1}\right)\left(\frac{k_{\mathrm{tcsc}}tan(k_{\mathrm{tcsc}}\beta_{\mathrm{tcsc}}) - tan\beta_{\mathrm{tcsc}}}{\pi}\right) \quad (19)$$

in which $\beta_{\mathrm{tcsc}} = \pi - \alpha_{\mathrm{tcsc}}$ is the angle of advance (before the forward voltage becomes zero) of the TCSC, α_{tcsc} is the firing angle of thyristors, $X_{C_\mathrm{tcsc}}$is the capacitive reactance of the TCSC, X_{L_tcsc} is the inductive reactance of the TCSC, and $k_{\mathrm{tcsc}} = \sqrt{X_{C\_\mathrm{tcsc}}/X_{L\_\mathrm{tcsc}}}$ is the compensation ratio of the TCSC. In order to prevent TCSC from operating in the resonance region, this study chooses the compensation ratio k_{tcsc} with the following constraint of $1 < k_{\mathrm{tcsc}} < 3$.

The control method: The TCSC controller's block diagram is depicted in Fig. 7 and is marked in pale blue color. The TCSC will be controlled using the fixed power method, and the control is

based on a PI algorithm. This systematic approach achieves the minimum settling time and ensures the quickest possible damping. The process optimizes the controller's performance in response to transient events. The power calculation block calculates the working power from the measured current and voltage data from the transmission line. The calculated power will be compared with the reference power value P_{ref} to obtain the error signal ΔP. This error signal goes through the PI controller, and the output signal of this PI controller will pass through the linear block and the α-limiting block ($\alpha_{tcsc\_min} = 90°$; $\alpha_{tcsc\_max} = 180°$) to create a signal supplied to the firing pulse generator block. Simultaneously, the pulse generator block will also receive the synchronized signal of the line current through the PLL block to synchronize the pulse signal [46], [48].

4.2. SVC

Structure and principle of operation: The SVC is one of the FACTS devices connected in parallel with the power system. It generates or absorbs continuous reactive power, operating within an unlimited range, with high-speed feedback control of power system parameters such as voltage. The SVC is primarily used in power systems to enhance voltage control and system stability [49]-[51].

The popular structure of the SVC is the fixed capacitor combined with the thyristor-switched capacitor (TSC) applied in this study, and the SVC is connected at the PCC, as illustrated in Fig. 8, and is marked in a pale yellow color [13], [52], in which a fixed capacitor is connected in parallel with the TCR. The TCR consists of a pair of anti-parallel thyristors connected in series with a reactor coil. The role of the thyristor pair is similar to a bidirectional switch. In the positive half-cycle, thyristor T_{1_svc} conducts, and in the negative half-cycle, thyristor T_{2_svc} conducts.

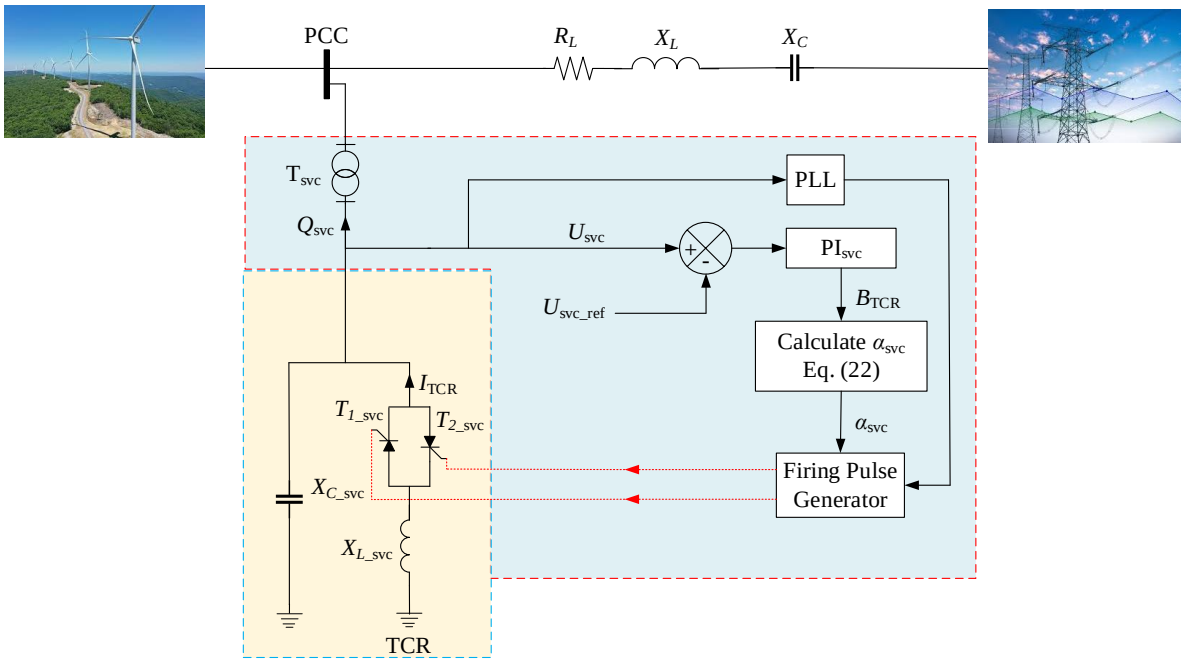

Fig. 8. The configuration and control method of SVC

The current equation of TCR is described as follows [13], [49], [53].

$$I_{TCR}(\alpha_{svc}) = U_{svc} B_{TCR}(\alpha_{svc}) \tag{20}$$

in which U_{svc} is the voltage at the connected SVC point, α_{svc} is the firing angle of the thyristors $\left(\frac{\pi}{2} \leq \alpha_{svc} \leq \pi\right)$, and B_{TCR} is the conductance of the TCR, which is determined as follows:

$$B_{TCR}(\alpha_{svc}) = \frac{2\pi - 2\alpha_{svc} + \sin 2\alpha_{svc}}{\pi X_{L\_svc}} \tag{21}$$

The reactive power, injecting at the installed SVC bus, is described as follows

$$Q_{\text{svc}} = U_{\text{svc}}^2 \left(\frac{\pi X_{L\_\text{svc}} - X_{\text{C\_svc}}(2\pi - 2\alpha_{svc} + \sin 2\alpha_{\text{svc}})}{\pi X_{C\_\text{svc}} X_{L\_\text{svc}}} \right) \quad (22)$$

where $X_{L_\text{svc}}$is the inductive reactance of the SVC and X_{C_svc} is the inductive reactance of the SVC.

The control method: The control scheme of the SVC, using the voltage control method, is depicted in Fig. 8 and is marked in pale blue color. The line voltage value is measured, and then it is compared with the reference voltage value to obtain the error signal ΔV. This signal passes through the voltage controller using the PI controller to generate TCR's field voltage signal B_{TCR}. The value of the firing angle α_{svc} is obtained from the TCR's field voltage signal B_{TCR} after passing through the angle calculation block using (22) along with the signal from the PLL block, providing the signal for the pulse generator to trigger TCR. The voltage control process continues iteratively until the measured voltage value matches the reference value, gradually damping the system oscillations through this process.

4.3. STATCOM

Structure and principle of operation: The STATCOM is a parallel-connected FACTS device capable of generating and absorbing reactive power with a controllable output that can be adjusted to control specific power system parameters. The STATCOM provides operating characteristics similar to a synchronous condenser but without mechanical inertia, as it utilizes power electronic devices such as GTO or IGBT for source conversion. Due to its parallel-connected structure, it offers fast control of three-phase voltage, both in magnitude and phase. The configuration includes parallel-connected transformers, a three-phase VSC, DC capacitor, and a controller linked to the VSC, as illustrated in Fig. 9, which is marked in pale yellow [54], [55].

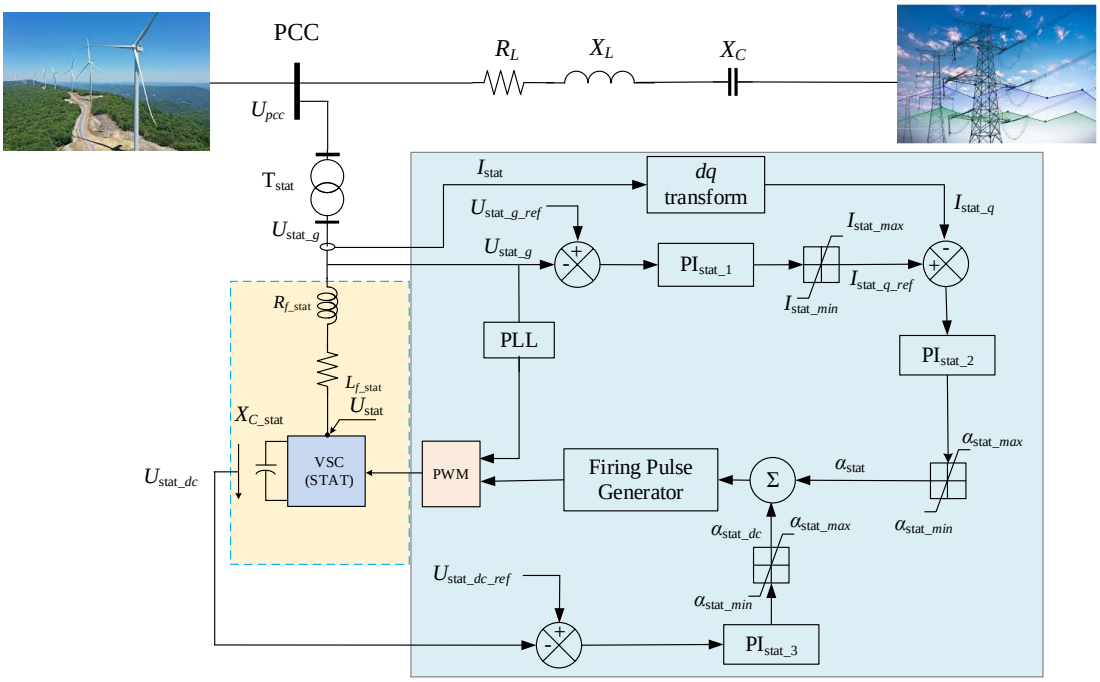

Fig. 9. The configuration of STATCOM

The control method: The control scheme of the control system of STATCOM, using the VSC, is illustrated in Fig. 9, and it is marked in pale blue color. This control aims to either supply or absorb reactive power to regulate the connection point voltage to the set voltage value $U_{\text{stat\_gref}}$. The decentralized control system relies on a full *dq* current control strategy, utilizing both the *d* and *q* components of the STATCOM current [15], [56].

The PLL synchronizes the phase of the voltage and three-phase current at the node where STATCOM is connected. The measured current signal from the STATCOM connection point is used to transform the *dq* components of the AC voltage and current. The voltage regulator receives signals from the measured voltage VS and the reference voltage U_{stat_gref} to calculate the reference current $I_{stat\_q\_ref}$. The measured current I_{stat} is transformed into I_{stat_q} through the *dq* transformation block. $I_{stat\_q\_ref}$ and I_{stat_q} are compared, and the error signal is passed through the current regulator to generate an α angle of the GTO voltage relative to the line voltage of the STATCOM bus. The pulse generator activates pulses for conversion from the output of the PLL and the output of the current regulator (by α).

While the STATCOM is operating, rapid changes in the voltage of the capacitor U_{stat_dc} may occur. To enhance the dynamic performance of the STATCOM controller, an additional DC voltage balancing controller is added using the capacitor U_{stat_dc} voltage signal. The U_{stat_dc} voltage is compared to the reference capacitor voltage, and if the deviation exceeds a threshold value, the additional DC balancing controller is activated. It generates a supplementary damping signal α_{dc} to trigger the pulse generator. The main idea is to keep the capacitor voltage at the desired level. This supplementary controller reduces the ripple during capacitor charging or discharging, improving the fast control capability of the STATCOM. This helps to mitigate SSR better.

5. Simulation Results

The modified IEEE First Benchmark model, illustrated in Fig. 1, replaces the synchronous generator with a 66 × 1.5 MW DFIG. This network is used to evaluate the effectiveness of TCSC, SVC, and STATCOM controllers in mitigating SSR caused by IGE in the DFIG system. All dynamic models are simulated in the MATLAB/Simulink environment, as depicted in Fig. 10. The simulations are conducted with a discrete time step of $T_s = 10^{-6}$ seconds and a fixed wind speed of 15 m/s.

The SSR mitigation capabilities of the proposed TCSC, SVC, and STATCOM controllers are assessed based on their ability to dampen oscillations in the WPGS-DFIG's electric torque, rotor speed, active power, terminal voltage, and DC link voltage. The evaluation is carried out under the following two scenarios:

Scenario 1: A sudden increase in the line's compensation level.

Scenario 2: A three-phase short circuit occurring at the point of common coupling (PCC) of the DFIG system, as shown in Fig. 10.

The simulation results presented below demonstrate the system's dynamic performance, including electric torque, terminal voltage, and DFIG output power.

5.1. Scenario 1

As is well-known, the voltage and power on a transmission line continuously fluctuate due to various factors, especially load changes. To ensure stable operation, the line's compensation must be adjusted accordingly. In this scenario, the system operates stably with a compensation level of 50%. At the 4-second mark, the compensation is suddenly increased to 70%, which represents the critical level capable of triggering the SSR phenomenon. This scenario is chosen to effectively evaluate the results of this study.

The system's performance is illustrated in Fig. 11. Observing the black dashed line in this figure reveals significant oscillations in electric torque, active power, terminal voltage, DC link voltage, and rotor speed. These oscillations grow in magnitude over time as the compensation level reaches 70% in the absence of FACTS controllers, ultimately leading to system instability.

In contrast, when the proposed FACTS controllers are applied, these oscillations are significantly dampened, quickly restoring the system's stability. As shown in Fig. 11 (a) and (b), the oscillations in electric torque and active power are sharply reduced within 0.5 seconds, demonstrating the excellent capability of the three FACTS controllers in mitigating SSR-induced fluctuations.

These fluctuations clearly reveal distinctions among the FACTS controllers. The STATCOM demonstrates superior performance by completely eliminating SSR within 0.5 seconds, whereas TCSCs and SVCs achieve the same result in 0.8 seconds. While the SVC effectively suppresses SSR, it leaves minor fluctuations in the system's electrical torque. However, these fluctuations are negligible and do not significantly impact overall system performance.

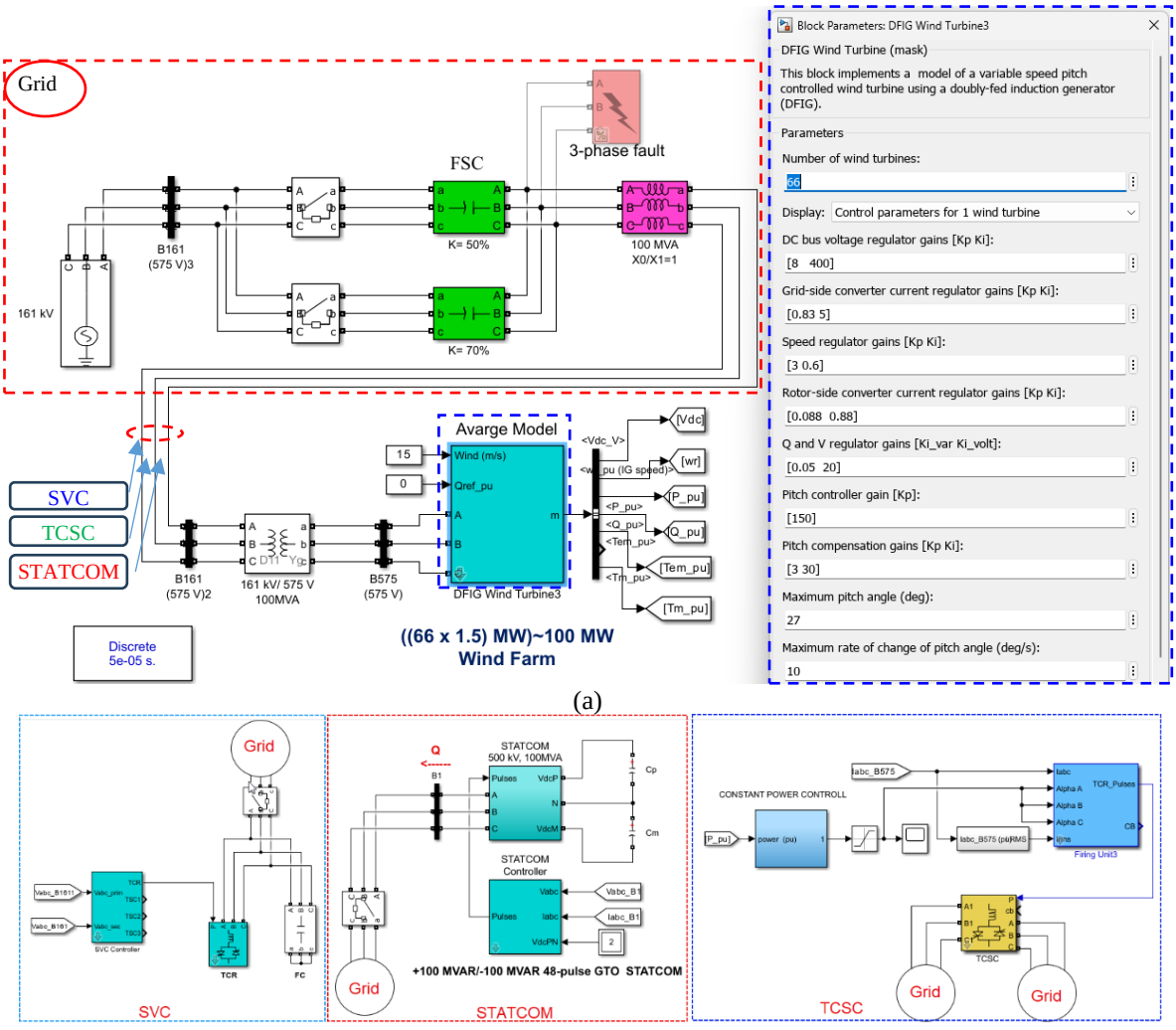

Fig. 10. The proposed test model for mitigating SSR using MATLAB/Simulink: (a) Grid-connected 66x1.5MW DFIG-turbine; (b) the grid-connected FACTS devices

Furthermore, Figs. 11 (d) and (e) indicate that the DC-link voltage and rotor speed stabilize when the compensation level reaches 70% with the application of FACTS devices. In contrast, without these devices, both parameters experience significant instability. Notably, Fig. 11 (e) highlights severe rotor speed deviations in the absence of FACTS adjustments, emphasizing their critical role in maintaining system stability.

A detailed comparison of the parameter amplitude values observed 5 seconds after the system re-stabilizes following the line compensation change is presented in Table 1. This comparison further highlights the effectiveness of FACTS solutions. The results confirm that the STATCOM controller plays a pivotal role in significantly mitigating the SSR phenomenon.

5.2. Scenario 2

This second operational scenario represents the worst-case condition for the system, involving a three-phase short-circuit fault at the PCC, occurring at the fourth second and lasting 75 ms. The

system operates at a normal compensation level, equivalent to 50% of the line compensation. The system response in this scenario is depicted in Fig. 12.

From the simulation results shown in Fig. 12 (a) - (c), it is observed that after the fault is cleared, for the case without FACTS devices (black-dashed line), the electrical torque, voltage, and output power of the DFIG increase rapidly over time. This can potentially lead to system shutdown and, in severe cases, cause significant damage to the wind turbine generator.

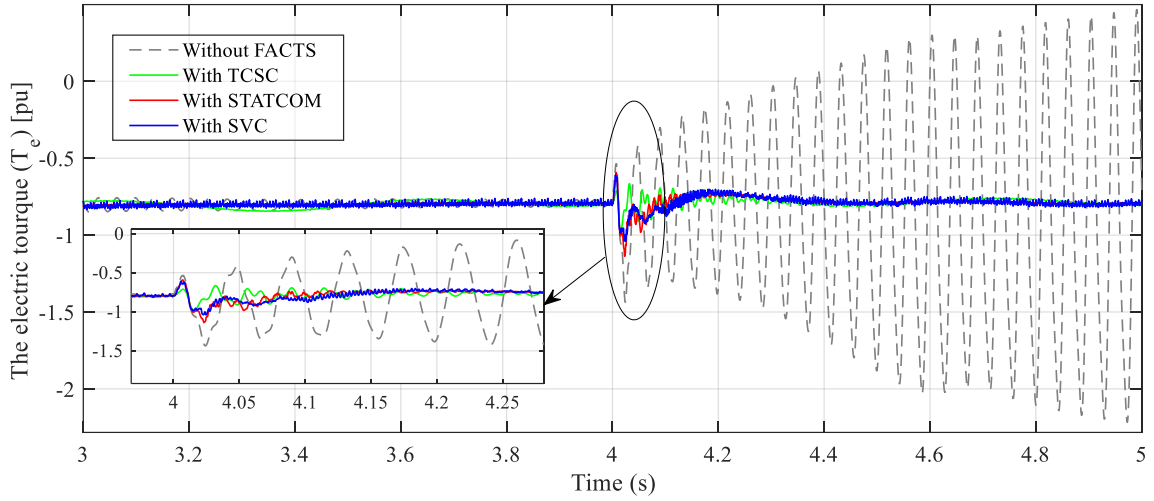

(a)

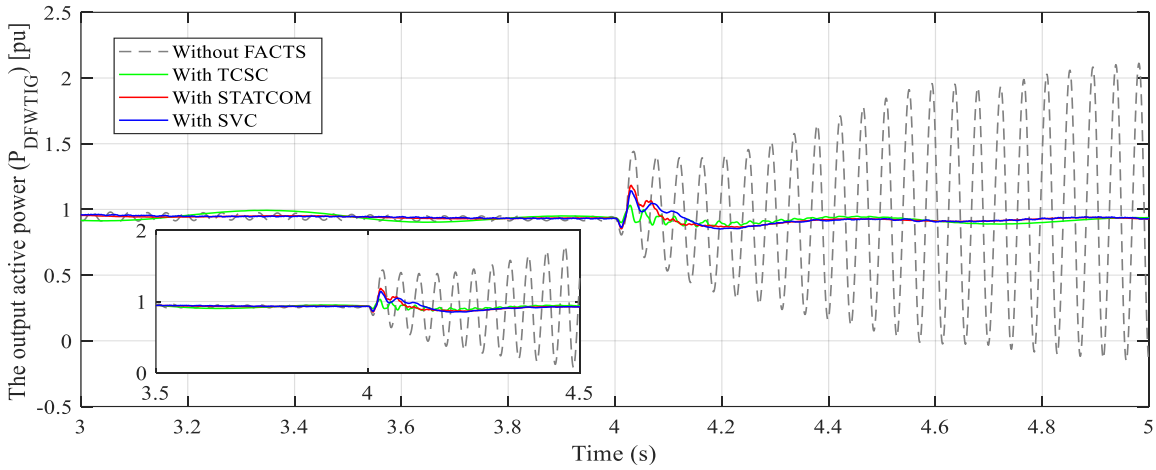

(b)

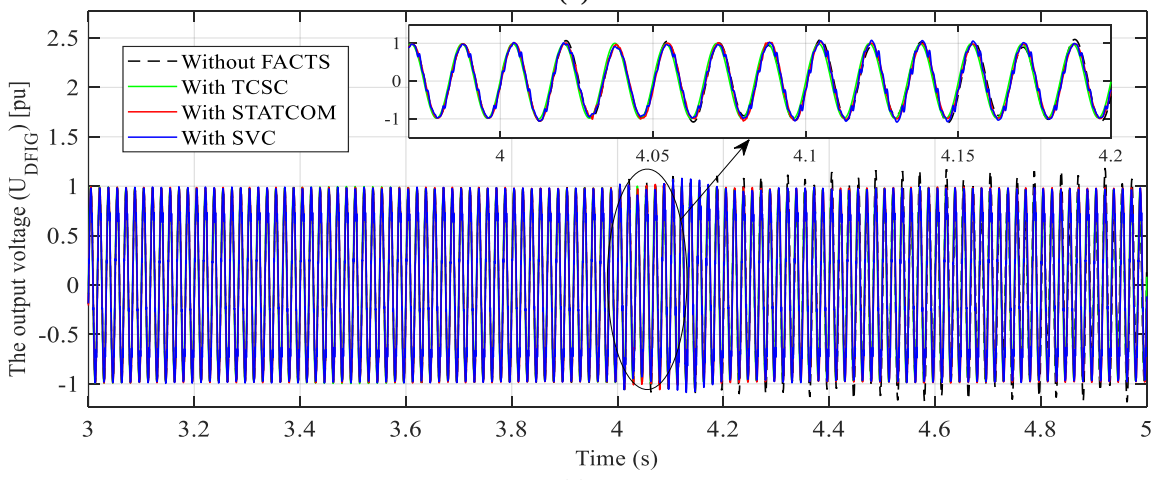

(c)

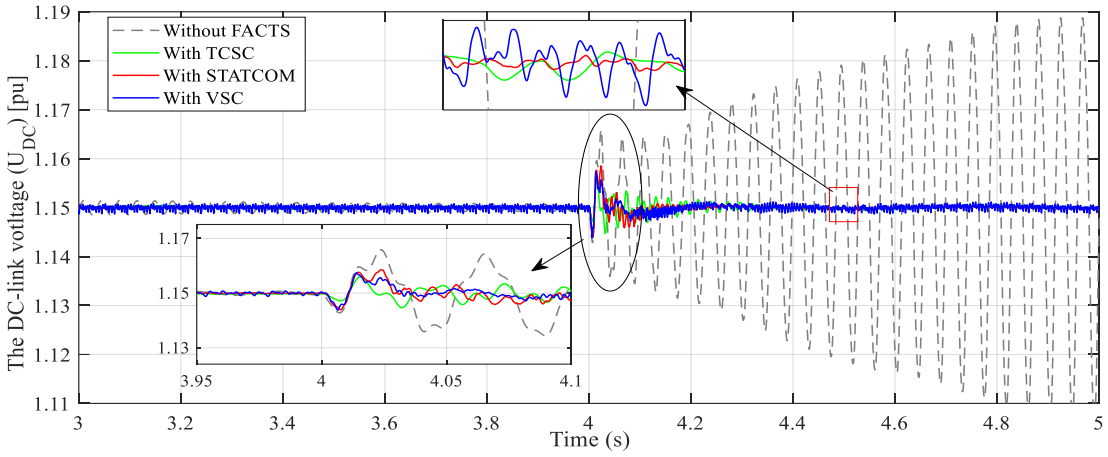

(d)

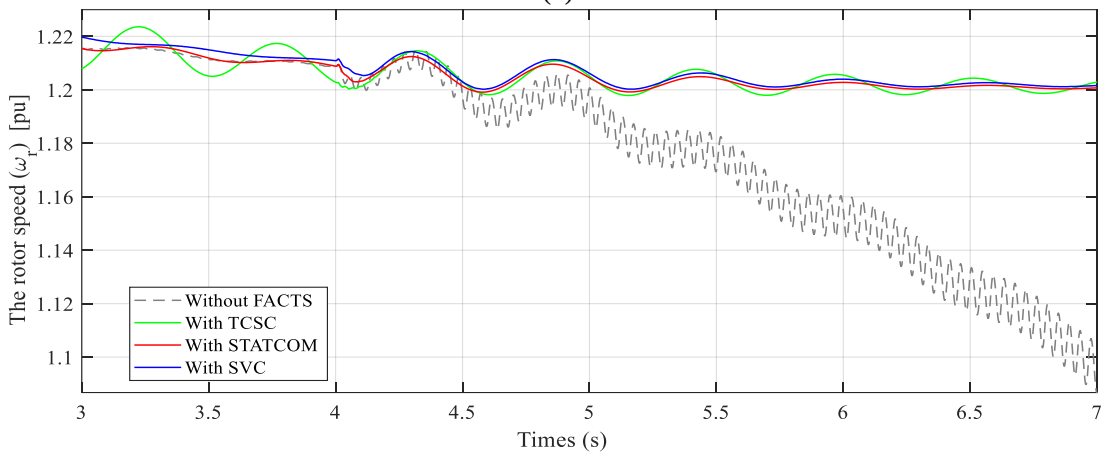

(e)

Fig. 11. The performance of the system under the condition of Scenario 1: (a) Electric torque, (b) Active power, (c) Stator voltage, (d) DC-link voltage, (e) Rotor speed

Table 1. Comparison of amplitude values of parameters at 5 seconds under scenario 1

Parameters	Without FACTS	With TCSC	With STATCOM	With SVC
The electric torque T_e (pu)	2.62	0.11	0.01	0.18
The terminal voltage V_{DFIG} (pu)	2.24	1.97	1.98	2.01
The active power P_{DFIG} (pu)	1.94	0.03	0.01	0.02
The DC link voltage V_{DC} (pu)	0.09	0.001	0.0004	0.0017
The rotor speed ω_r (pu)	inf	0.013	0.01	0.011

However, when FACTS devices such as TCSC (green line), SVC (blue line), or STATCOM (red line) are present, the oscillations in electrical torque and voltage of the wind power system are mitigated quickly. Specifically, the oscillations are eliminated approximately 0.5 seconds after fault clearance, demonstrating the effectiveness of all three devices in reducing SSR under worst-case operating conditions.

After the error occurs and resolves, the electrical torque oscillates continuously with a large amplitude and shows a tendency toward instability when FACTS devices are not used. However, incorporating an SVC controller stabilizes the system within 4.8 seconds. The TCSC controller achieves faster stabilization, taking 4.6 seconds, while the STATCOM controller demonstrates the most effective performance, stabilizing the electromagnetic torque within 4.3 seconds. This can be seen from Fig. 12 (a). As observed in Fig. 12 (b), when using STATCOM controllers, the terminal voltage oscillation rapidly stabilizes compared to TCSC and SVC controllers.

After recovering the grid fault, the output active power, depicted in Fig. 12 (c), experienced significant fluctuations in the absence of FACTS controllers, leading to operational instability. While applying the proposed FACTS controllers, the power fluctuations are significantly improved. When using the proposed TCSC, SVC, and STATCOM controllers, the active power values reach 2.45 pu, 2.3 pu, and 1.7 pu, respectively. Similarly, the DC-link voltage oscillation is significantly damped when using a STATCOM controller compared to not using a FACTS controller or the proposed TCSC and SVC controllers.

Fig. 12 (e) illustrates the rotor speed compared with or without using FACTS controllers. When no FACTS (dashed line) is applied, the rotor speed shows the largest oscillations, with peak values exceeding 1.26 pu and dipping below 1.18 pu, and it takes around 6 seconds to settle within an acceptable range. Among the proposed FACTS controllers, the STATCOM controller (red line) demonstrates the best performance, with oscillations limited to a narrow range between 1.21 pu and 1.23 pu, stabilizing completely by around 5 seconds. The VSC controller (blue line) reduces oscillations effectively but with a slightly larger range between 1.20 pu and 1.24 pu, and it takes slightly longer (about 5.5 seconds) to stabilize. The TCSC controller (green line) shows a moderate improvement, with oscillations ranging from 1.19 pu to 1.24 pu, but it takes nearly 6 seconds to stabilize, similar to the case without FACTS. Overall, the data clearly indicates that the proposed STATCOM controller provides the most effective damping of rotor speed oscillations and the quickest stabilization, making it the superior choice among the tested FACTS controllers.

A detailed comparison of the results in this scenario is summarized in Table 2. These results clearly demonstrate that the proposed STATCOM controller provides superior SSR mitigation performance compared to the other controllers.

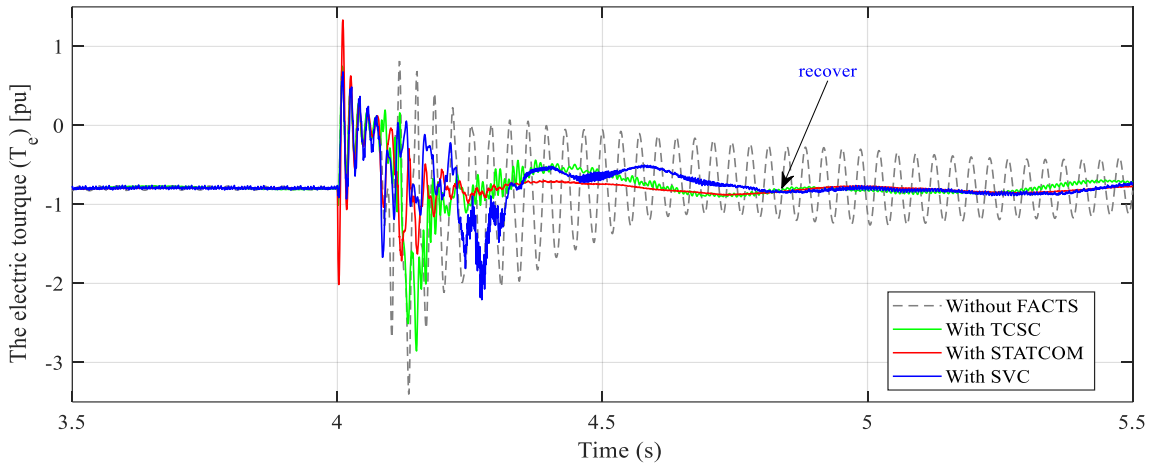

(a)

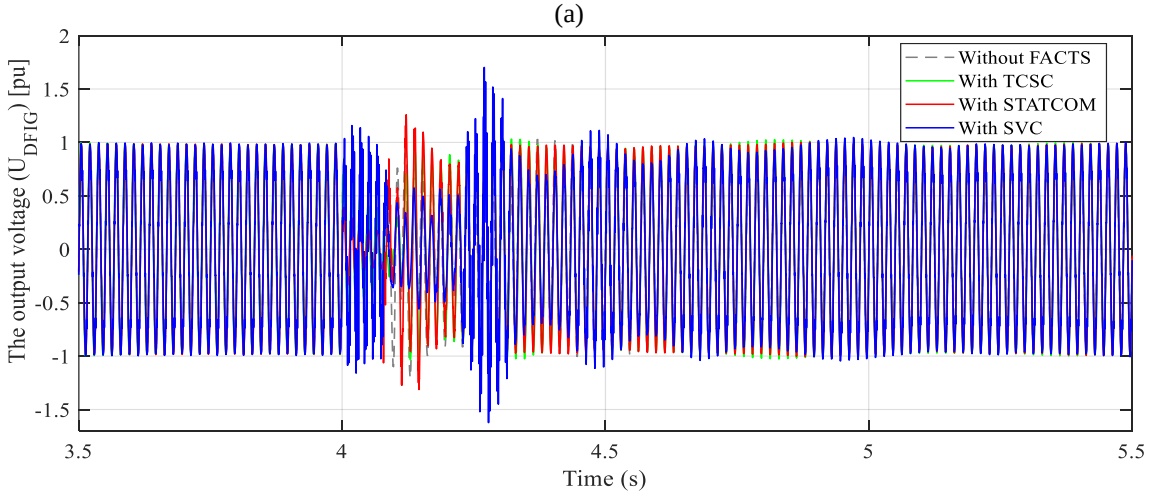

(b)

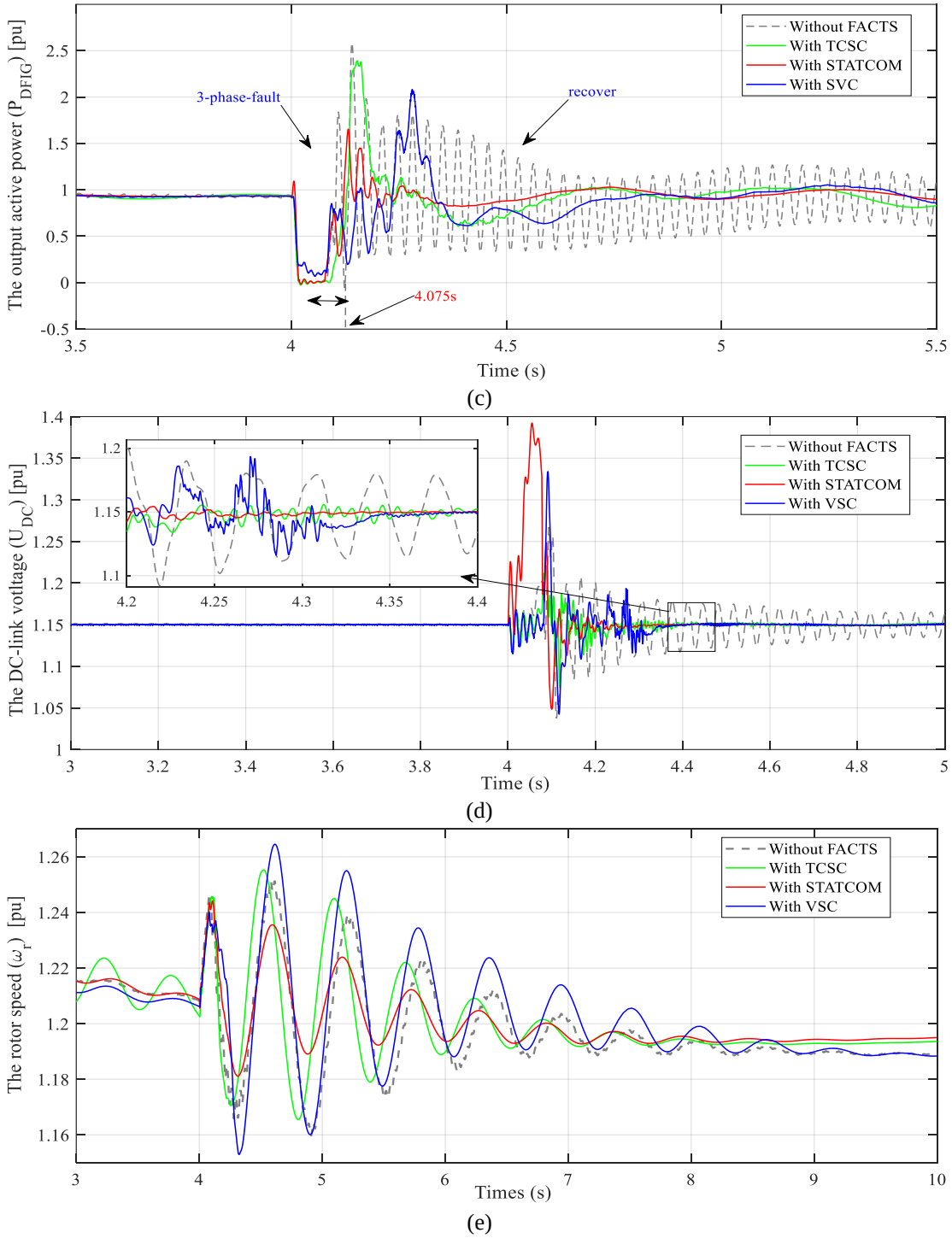

Fig. 12. The performance of the system under the condition of Scenario 2: (a) Electric torque, (b) Active power, (c) Stator voltage, (d) DC-link voltage, (e) Rortor speed

Table 2. Comparison of amplitude values of parameters at 5 seconds under scenario 2

Parameters	without FACTS	with TCSC	with STATCOM	with SVC
T_e (*pu*)	1.56	0.056	0.003	0.085
V_{DFIG} (*pu*)	1.757	1.907	1.952	2.021
P_{FIG} (*pu*)	1.75	0.117	0.009	0.149
V_{DC} (*pu*)	0.042	0.001	0.0003	0.001
ω_r (*pu*)	0.002	0.0001	0.0001	0.002

6. Conclusion

This paper investigates and compares the capabilities of FACTS devices in mitigating SSR caused by IGE in doubly fed wind turbine induction generators (DFWTIG) connected to compensated transmission lines. The study begins with a brief overview of the SSR phenomenon, followed by modeling the DFWTIG system using an equivalent impedance equation. A control strategy is proposed, incorporating RSC and GSC controllers based on a variable frequency converter. PI controllers are applied in the inner and outer loops to regulate the DC link voltage, grid voltage, electric torque, and reactive power, enabling independent control of active and reactive power while maintaining constant capacitor voltage. This ensures stable operation under short-circuit faults and varying compensation levels.

The paper also presents the structure and operating principles of TCSC, SVC, and STATCOM, with tailored control algorithms for regulating active and reactive power flow during three-phase faults or compensation level changes. Simulations are conducted using the modified IEEE First Benchmark model, where a 66 × 1.5 MW DFWTIG replaces the synchronous generator. Time-domain analysis under severe conditions, such as three-phase faults and maximum compensation levels, evaluates the SSR mitigation performance of TCSC, SVC, and STATCOM controllers.

The results confirm that all three controllers effectively reduce oscillations in the DFWTIG's electric torque, rotor speed, active power, terminal voltage, and DC link voltage. Among the devices, the STATCOM demonstrates superior SSR mitigation performance compared to TCSC and SVC, making it the most effective solution for enhancing system stability.

Author Contribution: All authors contributed equally to the main contributor to this paper. All authors read and approved the final paper.

Funding: This research received no external funding

Acknowledgment: The authors would like to thank the managers and the members of the "International Journal of Robotics and Control Systems (IJRCS)" for their precious remarks and suggestions.

Conflicts of Interest: The authors declare no conflict of interest.

References

[1] M. Elhindi, M. A. A. Abdalla, A. Omar, A. Pranolo, A. Mirghani, and A. A. Omer, "Comparative Electromagnetic Performance Analysis of Double Stator and Single Stator Superconducting Generators for Direct-Drive Wind Turbines," *International Journal of Robotics and Control Systems*, vol. 4, no. 2, pp. 678-690, 2024, https://doi.org/10.31763/ijrcs.v4i2.1385.

[2] N. Verma and N. Kumar, "DFIG-Based Wind Plant Coupled Series Compensated Transmission Line: Modeling and SSR Stability Analysis," *Journal of The Institution of Engineers*, vol. 103, no. 6, pp. 1917-1926, 2022, https://doi.org/10.1007/s40031-022-00807-6.

[3] R. Moreno-Sánchez, C. A. Núñez-Gutiérrez, N. Visairo-Cruz, J. Hernández-Ramírez and J. Segundo-Ramírez, "Understanding the Origin of SSR in Series-Compensated DFIG-Based Wind Farms: Analysis Techniques and Tuning," *IEEE Access*, vol. 9, pp. 117660-117672, 2021, https://doi.org/10.1109/ACCESS.2021.3104171.

[4] N. Verma, N. Kumar, S. Gupta, H. Malik, and F. P. G. Márquez, "Review of sub-synchronous interaction in wind integrated power systems: classification, challenges, and mitigation techniques," *Protection and Control of Modern Power Systems*, vol. 8, no. 2, pp. 1-26, 2023, https://doi.org/10.1186/s41601-023-00291-0.

[5] Z. Moradi-Shahrbabak, "Proposed sub-synchronous resonance damping controller for large-scale wind farms," *IET Renewable Power Generation*, vol. 17, no. 13, pp. 3209-3220, 2023, https://doi.org/10.1049/rpg2.12837.

[6] D. Fateh, A. A. M. Birjandi and J. M. Guerrero, "Safe Sub Synchronous Oscillations Response for Large DFIG-Based Wind Farms," *IEEE Access*, vol. 8, pp. 169822-169834, 2020, https://doi.org/10.1109/ACCESS.2020.3019234.

[7] D. Fateh, A. A. M. Birjandi, and J. M. Guerrero, "A subsynchronous resonance prevention for DFIG-based wind farms," *Turkish Journal of Electrical Engineering and Computer Sciences*, vol. 28, no. 5, pp. 2670-2685, 2020, https://doi.org/10.3906/elk-1912-177.

[8] X. Peng, R. Chen, J. Zhou, S. Qin, R. Bi, and H. Sun, "Research on Mechanism and Damping Control Strategy of DFIG-Based Wind Farm Grid-Connected System SSR Based on the Complex Torque Method," *Electronics*, vol. 10, no. 14, p. 1640, 2021, https://doi.org/10.3390/electronics10141640.

[9] L. Li, D. Zhu, X. Zou, J. Hu, Y. Kang, and J. M. Guerrero, "Review of frequency regulation requirements for wind power plants in international grid codes," *Renewable and Sustainable Energy Reviews*, vol. 187, p. 113731, 2023, https://doi.org/10.1016/j.rser.2023.113731.

[10] D. D. Tung, L. V. Dai, and C. L. Quyen, "Subsynchronous resonance and FACTS-novel control strategy for its mitigation," *Journal of Engineering*, vol. 2019, no. 1, pp. 1-14, 2019, https://doi.org/10.1155/2019/2163908.

[11] I. Y. Fawzy, M. A. Mossa, A. M. Elsawy, and A. A. Z. Diab, "Enhancing the Performance of Power System under Abnormal Conditions Using Three Different FACTS Devices," *International Journal of Robotics and Control Systems*, vol. 4, no. 1, pp. 1- 32, 2024, https://doi.org/10.31763/ijrcs.v4i1.1229.

[12] S. Impram, S. Varbak Nese, and B. Oral, "Challenges of renewable energy penetration on power system flexibility: A survey," *Energy Strategy Reviews*, vol. 31, p. 100539, 2020, https://doi.org/10.1016/j.esr.2020.100539.

[13] K. Gu, F. Wu, H. Zhen, Z. Wang, T. Niu and J. Li, "Comparative Study of the Impact of SVC on the SSR in DFIG-based Wind Farm Systems Under Different Series Compensation Levels," *2022 Power System and Green Energy Conference (PSGEC)*, pp. 342-346, 2022, https://10.1109/PSGEC54663.2022.9880998.

[14] Y. Zhang, C. Klabunde and M. Wolter, "Harmonic Resonance Analysis for DFIG-based Offshore Wind Farm with VSC-HVDC Connection," *2019 IEEE Milan PowerTech*, pp. 1-6, 2019, https://doi.org/10.1109/PTC.2019.8810495.

[15] M. I. Mosaad, H. S. M. Ramadan, M. Aljohani, M. F. El-Naggar and S. S. M. Ghoneim, "Near-Optimal PI Controllers of STATCOM for Efficient Hybrid Renewable Power System," *IEEE Access*, vol. 9, pp. 34119-34130, 2021, https://doi.org/10.1109/ACCESS.2021.3058081.

[16] D. R. Weerakoon, C. Karawita and U. D. Annakkage, "Evaluation of Inherent Damping Introduced by Thyristor Controlled Series Compensators," *IEEE Open Access Journal of Power and Energy*, vol. 10, pp. 259-269, 2023, https://doi.org/10.1109/OAJPE.2023.3247243.

[17] J. Samanes, E. Gubia, J. Lopez and R. Burgos, "Sub-Synchronous Resonance Damping Control Strategy for DFIG Wind Turbines," *IEEE Access*, vol. 8, pp. 223359-223372, 2020, https://doi.org/10.1109/ACCESS.2020.3043818.

[18] K. Okedu, M. Altobi, and S. Alaraimi, "Comparative Study of the Effects of Machine Parameters on DFIG and PMSG Variable Speed Wind Turbines during Grid Fault," *Frontiers in Energy Research*, vol. 9, pp. 174-187, 2021, https://doi.org/10.3389/fenrg.2021.681443.

[19] G. Ramya, P. Suresh, J. Jayashree, A. A. Charles and T. Daniya, "Review and Analysis of Techniques to Mitigate Sub Synchronous Resonance using FACTS Devices," *2022 International Virtual Conference on Power Engineering Computing and Control: Developments in Electric Vehicles and Energy Sector for Sustainable Future (PECCON)*, pp. 1-4, 2022, https://10.1109/PECCON55017.2022.9851163.

[20] Q. Li, W. Chen, Z. Wei, Z. Kang, Y. Tang, "Stability and modal analysis of a DFIG-based wind energy conversion system under stator voltage vector control," *International Journal of Electrical Power & Energy Systems*, vol. 162, p. 110286, 2024, https://doi.org/10.1016/j.ijepes.2024.110286.

[21] T. Engelbrecht *et al*., "STATCOM Technology Evolution for Tomorrow's Grid: E-STATCOM, STATCOM With Supercapacitor-Based Active Power Capability," *IEEE Power and Energy Magazine*, vol. 21, no. 2, pp. 30-39, 2023, https://doi.org/10.1109/MPE.2022.3230969.

[22] C. H. Ramalingegowda and M. Rudramoorthy, "Sub-synchronous resonance in wind energy integrated grid–problem and mitigation techniques–a review," *International Journal of Power Electronics and Drive Systems*, vol. 13, no. 3, pp. 1870-1886, 2022, http://doi.org/10.11591/ijpeds.v13.i3.pp1870-1886.

[23] Y. Wang, F. Chen, W. Jia, and R. Wang, "An Algorithm for Calculating the Parameter Selection Area of a Doubly-Fed Induction Generator Based on the Guardian Map Method," *Mathematics*, vol. 12, no. 7, p. 1044, 2024, https://doi.org/10.3390/math12071044.

[24] Z. Jian-hong, P. Zhang, X. Zhang, Q. Lin, C. Sun, and H. Li, "Model Predictive Control on Transient Flux Linkage and Reactive Power Compensation of Doubly Fed Induction Wind Generator," *International Journal of Energy Research*, vol. 2024, no. 1, pp. 1-15, 2024, https://doi.org/10.1155/2024/6648691.

[25] A. E. Leon and J. A. Solsona, "Sub-Synchronous Interaction Damping Control for DFIG Wind Turbines," *IEEE Transactions on Power Systems*, vol. 30, no. 1, pp. 419-428, 2015, https://doi.org/10.1109/TPWRS.2014.2327197.

[26] Y. Gong, Q. Huang, D.-S. Cai, and B. O. Olorunfemi, "Characteristics of sub-synchronous oscillation in grid-connected wind farm system," *Journal of Electronic Science and Technology*, vol. 21, no. 4, p. 100228, 2023, https://doi.org/10.1016/j.jnlest.2023.100228.

[27] V. D. Le, "Development of converter configuration and corresponding control strategy for wind turbines using permanent magnet synchronous generator: A Case study," *Journal of Energy Systems*, vol. 6, no. 4, pp. 484-502, 2022, https://doi.org/10.30521/jes.1025810.

[28] G. Yan, D. Wang, Q. Jia, and W. Hu, "Equivalent modeling of DFIG-based wind farms for sub-synchronous resonance analysis," *Energies*, vol. 13, no. 20, p. 5426, 2020, https://doi.org/10.3390/en13205426.

[29] L. V. Dai, "A novel protection method to enhance the grid-connected capability of DFIG based on wind turbines," *IETE Journal of Research*, vol. 70, no. 2, pp. 2047-2063, 2024, https://doi.org/10.1080/03772063.2022.2163925.

[30] L. Zhu, D. Zhong, B. Wang, R. Lin, and M. Xu, "Understanding subsynchronous oscillation in DFIG-based wind farms with rotor-side converter control based on the equivalent RLC model," *IEEE Access*, vol. 8, pp. 65371-65382, 2020, https://doi.org/10.1109/ACCESS.2020.2983727.

[31] V. Le, X. Li, Y. Li, T. L. T. Dong, and C. Le, "An innovative control strategy to improve the fault ride-through capability of DFIGs based on wind energy conversion systems," *Energies*, vol. 9, no. 2, p. 69, 2016, https://doi.org/10.3390/en9020069.

[32] N. Fahal and T. Zheng, "Control of DFIG-based wind power generation system under unbalanced grid voltage conditions," *Natural and Applied Sciences International Journal (NASIJ)*, vol. 5, no. 1, pp. 92-112, 2024, https://doi.org/10.47264/idea.nasij/5.1.7.

[33] F. Ameur, K. Kouzi, and K. Ameur, "Performance of New Control Strategy of Dual Stator Induction Generator System Applied in Wind Power Generation," *International Journal of Robotics and Control Systems*, vol. 4, no. 2, pp. 832-848, 2024, https://doi.org/10.31763/ijrcs.v4i2.1404.

[34] H. Benbouhenni *et al*., "Dynamic performance of rotor-side nonlinear control technique for doubly-fed multi-rotor wind energy based on improved super-twisting algorithms under variable wind speed," *Scientific Reports*, vol. 14, no. 1, p. 5664, 2024, https://doi.org/10.1038/s41598-024-55271-7.

[35] Y. Moumani, A. J. Laafou, and A. A. Madi, "A comparative study based on proportional integral and backstepping controllers for doubly fed induction generator used in wind energy conversion system," *Archives of Electrical Engineering*, vol. 72, no. 1, pp. 211-228, 2023, https://doi.org/10.24425/aee.2023.143698.

[36] J. Pedra, L. Sainz, and L. Monjo, "Impact of Short-Circuit Ratio on Control Parameter Settings of DFIG Wind Turbines," *Energies*, vol. 17, no. 8, p. 1825, 2024, https://doi.org/10.3390/en17081825.

[37] S. Rezaei, S. Aref, and A. Sedighi Anaraki, "A review on oscillations in Wind Park due to ferroresonance and subsynchronous resonance," *IET Renewable Power Generation*, vol. 15, no. 16, pp. 3777-3792, 2021, https://doi.org/10.1049/rpg2.12287.

[38] A. K. Abdulabbas, S. M. Salih, and M. A. Alawan, "The Analysis of Sub-Synchronous Resonance in a Wind Farm for a Doubly-Fed Induction Generator Using Modern Analytical Method," *Iraqi Journal for*

Electrical and Electronic Engineering, vol. 20, no. 1, pp. 257-270, 2024, https://doi.org/10.37917/ijeee.20.1.24.

[39] S. Velpula, R. Thirumalaivasan and M. Janaki, "Stability Analysis on Torsional Interactions of Turbine-Generator Connected With DFIG-WECS Using Admittance Model," *IEEE Transactions on Power Systems*, vol. 35, no. 6, pp. 4745-4755, 2020, https://doi.org/10.1109/TPWRS.2020.2992111.

[40] M. Abdeen *et al.*, "A Recent Analytical Approach for Analysis of Sub-Synchronous Resonance in Doubly-Fed Induction Generator-Based Wind Farm," *IEEE Access*, vol. 9, pp. 68888-68897, 2021, https://doi.org/10.1109/ACCESS.2021.3075965.

[41] Z. Liu, D. Li, W. Wang, J. Wang, and D. Gong, "A Review of the Research on the Wide-Band Oscillation Analysis and Suppression of Renewable Energy Grid-Connected Systems," *Energies*, vol. 17, no. 8, p. 1809, 2024, https://doi.org/10.3390/en17081809.

[42] H. Noh, H. Cho, S. Choi, and B. Lee, "Mitigating Subsynchronous Torsional Interaction Using Geometric Feature Extraction Method," *Sustainability*, vol. 14, no. 23, p. 16110, 2022, https://doi.org/10.3390/su142316110.

[43] X. Yuan *et al.*, "An Effective Control Scheme for Multimodal SSR Suppression via VSC-Based Controller," *IEEE Access*, vol. 8, pp. 172581-172592, 2020, https://doi.org/10.1109/ACCESS.2020.3025152.

[44] G. Moustafa, M. A. Tolba, A. M. El-Rifaie, A. Ginidi, A. M. Shaheen, and S. Abid, "A Subtraction-Average-Based Optimizer for Solving Engineering Problems with Applications on TCSC Allocation in Power Systems," *Biomimetics*, vol. 8, no. 4, p. 332, 2023, https://doi.org/10.3390/biomimetics8040332.

[45] P. Singh, R. Tiwari, V. Sangwan and A. K. Gupta, "Optimal Allocation of Thyristor-Controlled Series Capacitor (TCSC) and Thyristor-Controlled Phase-Shifting Transformer (TCPST)," *2020 International Conference on Power Electronics & IoT Applications in Renewable Energy and its Control (PARC)*, pp. 491-496, 2020, https://doi.org/10.1109/PARC49193.2020.236662.

[46] K. Dey, M. K. Das, and A. M. Kulkarni, "Comparison of dynamic phasor, discrete-time and frequency scanning based SSR models of a TCSC," *Electric Power Systems Research*, vol. 196, p. 107237, 2021, https://doi.org/10.1016/j.epsr.2021.107237.

[47] V. Le, X. Li, and C. Le, "A novel method for seeking optimal placement of TCSC to damp oscillations in power systems," *International Journal of Control and Automation*, vol. 8, no. 4, pp. 333-346, 2015, https://doi.org/10.14257/ijca.2015.8.4.31.

[48] V. S. Patil and M. P. Thakre, "Assessment & Alternatives for SSR in a Series Capacitor Wind Farm Employing TCSC," *Journal of Physics: Conference Series*, vol. 1917, no. 1, p. 012004, 2021, https://doi.org/10.1088/1742-6596/1917/1/012004.

[49] A. Bhandakkar and L. Mathew, "Real-Time Simulation of Static VAR Compensator and Static Synchronous Compensator," *International Journal of Recent Technology and Engineering (IJRTE)*, vol. 8, no. 6, pp. 1950-1958, 2020, http://www.doi.org/10.35940/ijrte.F8047.038620.

[50] V. D. Le, X. Li, P. Li, and C. Q. Le, "A novel approach for determining optimal number and placement of static var compensator device to enhance the dynamic performance in power systems," *Electrical Engineering*, vol. 100, no. 3, pp. 1517-1533, 2018, doi: https://doi.org/10.1007/s00202-017-0598-z.

[51] V. Le, X. Li, Y. Li, Y. Cao, and C. Le, "Optimal placement of TCSC using controllability Gramian to damp power system oscillations," *International Transactions on Electrical Energy Systems*, vol. 26, no. 7, pp. 1493-1510, 2016, https://doi.org/10.1007/s00202-017-0598-z.

[52] A. Farah *et al.*, "A New Design Method for Optimal Parameters Setting of PSSs and SVC Damping Controllers to Alleviate Power System Stability Problem," *Energies*, vol. 14, no. 21, p. 7312, 2021, https://doi.org/10.3390/en14217312.

[53] L. V. Dai, X. Li, P. Li, and L. C. Quyen, "An optimal location of static VAr compensator based on Gramian critical energy for damping oscillations in power systems," *IEEJ Transactions on Electrical and Electronic Engineering*, vol. 11, no. 5, pp. 577-585, 2016, https://doi.org/10.1002/tee.22275.

[54] H. Noh, H. Cho, S. Lee, and B. Lee, "STATCOM with SSR damping controller using geometric extraction on phase space reconstruction method," *International Journal of Electrical Power & Energy Systems*, vol. 120, p. 106017, 2020, https://doi.org/10.1016/j.ijepes.2020.106017.

[55] L. V. Dai, D. D. Tung, and L. C. Quyen, "A highly relevant method for incorporation of shunt connected FACTS device into multi-machine power system to dampen electromechanical oscillations," *Energies*, vol. 10, no. 4, p. 482, 2017, https://doi.org/10.3390/en10040482.

[56] K. D. E. Kerrouche, E. Lodhi, M. B. Kerrouche, L. Wang, F. Zhu, and G. Xiong, "Modeling and design of the improved D-STATCOM control for power distribution grid," *SN Applied Sciences*, vol. 2, 2020, https://doi.org/10.1007/s42452-020-03315-8.